Electronic Spectra of Linear Isoelectronic Clusters $C_{2n+1}S$ and $C_{2n+1}Cl^+$ ($n = 0-4$): An ab Initio Study

Jinglai Zhang,[†] Wenpeng Wu,[†] Lianbin Wang,[†] Xing Chen,[‡] and Zexing Cao*[,‡]

Institute of Fine Chemistry and Engineering, Henan University, Kaifeng 475001, China, and the State Key Laboratory of Physical Chemistry of Solid Surfaces and Department of Chemistry, Xiamen University, Xiamen 361005, China

Received: May 21, 2006; In Final Form: July 5, 2006

Structures and stabilities of linear carbon chains $C_{2n+1}S$ and $C_{2n+1}Cl^+$ (n=0−4) in their ground states have been investigated by the CCSD and B3LYP approaches. The CASSCF calculations have been used to determine geometries of selected excited states of both isoelectronic series. Linear $C_{2n+1}S$ cluster has a cumulenic carbon framework, whereas its isoelectronic $C_{2n+1}Cl^+$ has a dominant character of acetylenic structure in the vicinity of terminal Cl. The vertical excitation energies of low-lying excited states have been calculated by the CASPT2 method. Calculations show that the excitation energies have nonlinear size dependence. The $2^1\Sigma^+ \leftarrow X^1\Sigma^+$ transition energy in $C_{2n+1}S$ has a limit of 1.78 eV, as the chain size is long enough. The predicted vertical excitation energies for relatively strong $1^1\Pi \leftarrow X^1\Sigma^+$ and $2^1\Sigma^+ \leftarrow X^1\Sigma^+$ transitions are in reasonable agreement with available experimental values. The spin−orbit effect on the spin-forbidden transition in both series is generally small, and the enhancement of the spin-forbidden transition by spin−orbit coupling exhibits geometrical and electronic structural dependence.

I. Introduction

In the past several decades, there has been a growing interest in experimental and theoretical studies of pure carbon clusters and heteroatom-terminated carbon clusters, because of significant interest in nanotechnology and astrochemistry, as well as their potential applications as building components of molecular materials in molecular electronics.[1−13] Among the heteroatom-containing carbon clusters, the sulfur- and chlorine-terminated carbon clusters have attracted considerable attention due to their relevance in the interstellar medium.[14−37]

The sulfur-terminated carbon-chain molecules C_nS ($n = 1-5$) species have been detected in dense interstellar clouds on the basis of laboratory microwave data, and the gas-phase rotational spectra of larger chains C_nS ($n = 4-9$) have also been reported.[14] In argon matrixes, some infrared vibrations of asymmetric and symmetric carbon−sulfur clusters C_nS and SC_nS ($n = 1-5$) have been observed, and they have been assigned by a combination of isotopic ($^{12}C/^{13}C$) substitution and theoretical calculations.[15] For C_nS ($n = 2-9$), vibrational frequencies and bonding features in their ground states have been determined theoretically.[16] Recently, density functional theory (DFT) calculations have been used to investigate vibrational frequencies and dissociation channels of larger linear carbon−sulfur clusters C_nS_m ($n = 1-29$, $m = 1-2$).[17,18] The structural and energetic properties of the low-lying excited states of C_nS have been investigated by electronic spectroscopy in the gas phase for C_2S[19] and in neon matrixes for C_2S/C_2S^-,[20] C_4S/C_4S^-,[21] C_5S, and C_6S/C_6S^-.[22]

Among the chlorine-capped carbon-chain compounds, the spectra of CCl radical have been reported in the ultraviolet,[23−25] microwave,[26] and infrared[27−29] regions. High-resolution gas-phase spectroscopic studies have been conducted for CCl^+ cation.[30] The triatomic radical C_2Cl has been investigated via a combination of microwave spectroscopy and ab initio calculations.[31] The electronic structures, dipole moments, and vibrational frequencies of the chlorine-terminated clusters C_nCl, C_nCl^+, and C_nCl^- ($n = 1-7$) have been determined at the B3LYP/6-311G(d) level,[32,33] and the lowest-energy states of all species but C_3Cl have either linear or quasilinear structures. On the basis of DFT calculations, Li and Tang[34] have predicted the ground-state electronic structures, incremental binding energies, ionization potentials, and electronic affinities for the second-row-atom-doped linear carbon clusters $C_nX/C_nX^{\pm}$ ($n = 1-10$; X = Na, Mg, Al, Si, P, S, or Cl). The results reveal that the odd−even effects in their stabilities arise from the numbers of the valence π electrons.

The electronic absorption spectra of $C_3Cl/C_3Cl^{\pm}$, C_4Cl, and C_4Cl^+ have been recorded in 6 K neon matrixes through mass selection technique.[35] The band systems of linear C_3Cl^+ appear at 413.2 nm, corresponding to the $^1\Pi \leftarrow X^1\Sigma^+$ transition. The electronic absorption spectra of C_5Cl, C_6Cl, C_5Cl^+, and C_6Cl^+ have also been recorded in neon matrixes.[36] The observed spectra with band origin at 266.1 nm are assigned to the $^1\Sigma^+ \leftarrow X^1\Sigma^+$ electronic transition in C_5Cl^+.

Among the observed electronic spectra of these sulfur-terminated and chlorine-terminated carbon clusters, only quite few bands were relatively well interpreted. A thorough understanding of the excited-state properties is important for material science, luminescence, and chemistry of the interstellar medium. In our previous studies,[37] the electronic spectra of even-numbered carbon chains $C_{2n}S$ and $C_{2n}Cl^+$ ($n = 1-5$) have been calculated in detail. In the present work, we will extend our study to the odd-numbered clusters $C_{2n+1}S$ and $C_{2n+1}Cl^+$ ($n = 0-4$), and equilibrium geometries, vertical excitation energies, and spin-forbidden transitions of these linear isoelectronic carbon clusters have been explored theoretically.

* Corresponding author. Electronic mail: zxcao@xmu.edu.cn.
[†] Henan University.
[‡] Xiamen University.

10.1021/jp063109n CCC: $33.50
Published on Web 08/05/2006

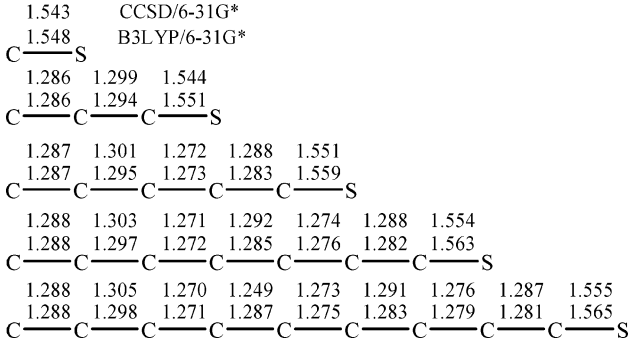

Figure 1. The optimized bond lengths (in Å) of linear S-terminated chains $C_{2n+1}S$ ($n = 0-4$).

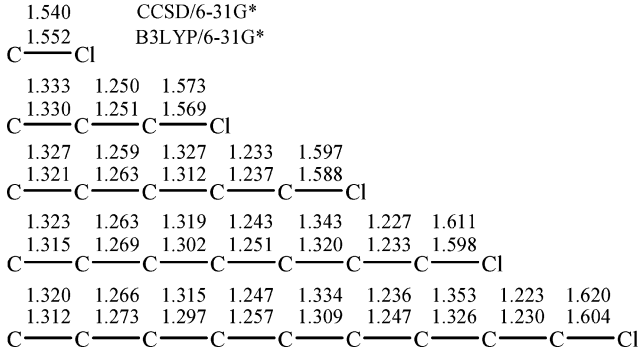

Figure 2. The optimized bond lengths (in Å) of linear Cl-terminated chains $C_{2n+1}Cl^+$ ($n = 0-4$).

II. Computational Details

Coupled cluster (CCSD)[38] and B3LYP[39−41] calculations with the 6−31G* basis set have been used to determine equilibrium geometries of the linear chains $C_{2n+1}S$ and $C_{2n+1}Cl^+$ ($n = 0-4$) in their ground states. Rotational constants and dipole moments have also been estimated in calculation. The nature of optimized structures has been assessed by frequency calculation.

The relative energies of the low-lying states of linear clusters $C_{2n+1}S$ and $C_{2n+1}Cl^+$ ($n = 0-4$) have been calculated by the complete-active-space-perturbation-second-order-theory (CASPT2) method[42] with the cc-pvTZ basis set at the CCSD/6-31G* optimized geometry. In the CASPT2 calculation, the CASSCF active spaces are generally composed of 18 electrons in 12 orbitals for all species except C_3S and C_3Cl^+ (14 electrons in 10 orbitals). The oscillator strengths (*f*) are calculated with the following formula:

$$f = \frac{2}{3}\Delta E|TM|^2 \qquad (1)$$

where ΔE is the transition energy between the ground state and the excited state in atomic unit, and TM is the transition moment in atomic unit. The spin−orbit coupling among perturbing singlet and triplet states has been estimated by the spin−orbit coupling configuration interaction (SOC−CI) calculation[43] with the 6-31G* basis set.

The CASSCF (14,10)[44,45] calculation has been used for full geometry optimization of the excited state $2^1\Sigma^+$ of $C_{2n+1}S$ and $C_{2n+1}Cl^+$ ($n = 1-4$). After the excited states were located, vertical emission energies have been calculated by CASPT2 calculations with the cc-pvTZ basis set. The active space is the same with that in calculation of vertical excitation energy.

All calculations have been performed by GAUSSIAN 98[46] and MOLPRO 2002[47] program packages.

III. Results and Discussion

A. Geometries and Stabilities of the Linear Chains. The B3LYP-optimized bond lengths of linear $C_{2n+1}S$ ($n = 0-4$) chains in their ground states are displayed in Figure 1. For comparison, the CCSD-optimized geometries are incorporated into Figure 1. As Figure 1 shows, the optimized geometries by different methods are quite similar. In comparison with the available experimental values, the present calculations predicted reliable equilibrium geometries. For instance, C_3S has experimental CC and CS bond lengths of 1.272, 1.303, and 1.532 Å,[48] and CS has experimental bond length of 1.535 Å.[49] Corresponding CCSD-optimized bond lengths have an accuracy of no more than 0.014 Å. Apparently, All carbon−carbon bond lengths are comparable with the maximum deviation 0.027 Å in $C_{2n+1}S$ ($n = 0-4$), showing a character of cumulenic structure in these carbon chains. This differs from $SC_{2n}S^{2-}$,[50] but similar to $C_{2n}S$[37] and $SC_{2n}S$.[15,51] As the number of carbon atoms increase from 1 to 9, the length of carbon−sulfur bond increases slightly from 1.548 to 1.565 Å.

The CCSD- and B3LYP-optimized bond lengths of linear $C_{2n+1}Cl^+$ ($n = 0-4$) chains in their ground states are shown in Figure 2. Both CCSD and B3LYP calculations predict almost the same geometries. As the chain elongates, the bond length of C−Cl increases from 1.552 Å ($n = 0$) to 1.604 Å ($n = 4$). Unlike $C_{2n+1}S$, the CC bond lengths in Figure 2 indicate that there is a character of bond length alternation, especially in the vicinity of the chlorine terminal. Such difference in the bond length distribution implies that there are different bonding properties in both isoelectronic series. Actually, the pure odd-numbered carbon chain has a closed-shell ground state with a cumulenic bonding character, e.g. a : C=C=C···C=C: structure for C_{2n+1}. Adduction of S to the carbon chain results in : C=C=C···C=C−S, and the bonding in the carbon chain subunit is still unchanged. In contrast, the acetylenic bonding can disperse the positive charge in $C_{2n+}1Cl^+$ through conjugation interaction and it will stabilize the cationic cluster. Presumably, this difference in bonding between both isoelectronic series may cause distinct properties of their low-lying excited states.

Table 1 lists the calculated rotational constants B_e and dipole moments μ for $C_{2n+1}S$ and $C_{2n+1}Cl^+$ ($n = 0-4$), and the available experimental values are also presented for comparison. As Table 1 displays, the rotational constants determined by CCSD and B3LYP are very close. It can be seen that the predicted values show good agreement with the experimental values,[14,52−56] indicating that present optimized geometries of these chains in their ground states are reliable. For example, the predicted rotational constant of C_9S is 220.97 MHz by B3LYP and 220.06 MHz by CCSD, in consistent with the observed value of 222.72 MHz. The predicted dipole moments increase monotonically as the chain lengthens, in agreement with previous studies.[17] It is noticeable that the dipole moments of $C_{2n+1}S$ are generally significantly larger than those of C_{2n+1}-Cl^+.

Tables 2 and 3 compile vibrational frequencies of linear $C_{2n+1}S$ and $C_{2n+1}Cl^+$ species by B3LYP. Frequency calculations show that both chains are stable structures on the potential energy surfaces without imaginary frequency. These linear structures in their ground states have been explored in previous studies.[17,18,34] Experimentally, a few strong bands attributed to the stretching mode of the C−S and C−C bonds in $C_{2n+1}S$ have been observed. For example, the strong absorptions of C−S bond in CS and C_3S occur at 1275 and 1534 cm^{-1},[15,57−59] respectively. Present B3LYP calculations predict that such C−S stretching frequencies appear at 1289 and 1567 cm^{-1}, respec-

TABLE 1: Predicted Rotational Constants B_E (in MHz) and Dipole Moments μ (in Debye) of $C_{2n+1}S$ and $C_{2n+1}Cl^+$ ($n = 0-4$) by B3LYP and CCSD Approaches

	B_e			m		B_e		m
species	B3LYP	CCSD	expt.[a]	B3LYP	species	B3LYP	CCSD	B3LYP
CS	24184.42	24306.72	24495.50	1.5192	CCl^+	23471.19	23752.43	0.0539
C_3S	2858.96	2858.35	2890.38	3.0405	C_3Cl^+	2751.40	2728.21	0.4766
C_5S	914.06	912.02	922.70	4.0296	C_5Cl^+	878.44	867.17	0.7016
C_7S	410.93	409.53	414.43	4.9647	C_7Cl^+	395.43	389.56	1.0067
C_9S	220.97	220.06	222.72	5.8706	C_9Cl^+	213.14	209.91	1.3075

[a] Refs 14 and 52−56.

TABLE 2: Calculated Harmonic Virbrational Frequencies (in cm^{-1}) of $C_{2n+1}S$ in Their Ground States by B3LYP/6-31G*

species	mode	vibrational frequencies								
CS	σ	1289								
	expt[a]	1275								
C_3S	π	186	513							
	σ	740	1567	2159						
	expt[a]	726	1534	2048						
C_5S	π	94	248	459	638					
	σ	546	1094	1662	2097	2253				
	expt[a]					2125				
C_7S	π	56	152	282	442	551	752			
	σ	435	859	1290	1720	2021	2223	2240		
C_9S	π	37	101	193	300	435	508	617	848	
	σ	361	712	1063	1413	1744	2004	2123	2206	2268

[a] Experimental values from refs 15 and 57−59.

TABLE 3: Calculated Harmonic Virbrational Frequencies (in cm^{-1}) of $C_{2n+1}Cl^+$ in Their Ground States by B3LYP/6-31G*

species	mode	vibrational frequencies								
CCl^+	σ	1172								
C_3Cl^+	π	140	404							
	σ	689	1455	2232						
	expt[a]			2143						
C_5Cl^+	π	86	206	330	588					
	σ	513	1037	1566	2182	2291				
C_7Cl^+	π	55	137	239	295	499	687			
	σ	412	817	1231	1634	2121	2252	2282		
C_9Cl^+	π	37	97	170	241	308	460	594	794	
	σ	345	680	1020	1355	1670	2095	2180	2237	2298

[a] Experimental value from ref 60.

tively. As Tables 2 and 3 display, calculated frequencies are in good agreement with available experimental values.

B. Vertical Excitation Energies of Singlet States. *Energies of Singlet Excited States in $C_{2n+1}S$.* The linear $C_{2n+1}S$ clusters have the closed-shell electronic configuration: [core] $(2n+5)\sigma^2 \cdots (4n+6)\sigma^2\, 2\pi^4 \cdots (n+1)\pi^4\, (4n+7)\sigma^2\, (n+2)\pi^4\, (n+3)\pi^0$, where the core contains $4n+8$ σ electrons and four π electrons. Such configuration will give rise to the singlet ground state of $^1\Sigma^+$. The low-lying states from $\pi\rightarrow$p and $\sigma\rightarrow$p excitations have been investigated in the present work.

The CASPT2 vertical transition energies (ΔE) and oscillator strengths (f) of $C_{2n+1}S$ ($n = 0-4$) for the electronic excitations to the singlet excited states are listed in Table 4. The low-lying states of $^1\Sigma^+$, $^1\Pi$, $^1\Sigma^-$, and $^1\Delta$ have been considered. For comparison, available experimental values of vertical transition energies are incorporated into Table 4.

As Table 4 shows, the predicted excitation energies agree with observed values. For example, the lowest excited state $1^1\Pi$ of CS, arising from the electronic promotion from 7σ to 3π, lies at 4.92 eV above the ground state, with an oscillator strength of 1.35×10^{-2}, in good agreement with the experimental value of 4.81 eV. The next low-lying states are $1^1\Sigma^-$ and $1^1\Delta$ from

TABLE 4: Calculated Vertical Excitation Energies ΔE (in eV) and Oscillator Strengths f of the Singlet Excited States in $C_{2n+1}S$ ($n = 0-4$) by CASPT2

n	state	transition	ΔE	f
0	$X^1\Sigma^+$	$\cdots 2\pi^4 7\sigma^2 3\pi^0$	0.00	
	$1^1\Pi$	$7\sigma \rightarrow 3\pi$	4.92 (4.81)[a]	1.35×10^{-2}
	$1^1\Sigma^-$	$2\pi \rightarrow 3\pi$	5.73	0
	$1^1\Delta$	$2\pi \rightarrow 3\pi$	5.80	0
	$2^1\Sigma^+$	$2\pi \rightarrow 3\pi$	8.14	1.52×10^{-1}
	$2^1\Pi$	$2\pi 7\sigma \rightarrow 3\pi^2$	9.01	9.01×10^{-2}
	$3^1\Sigma^+$	$7\sigma^2 \rightarrow 3\pi^2$	9.77	3.59×10^{-3}
	$2^1\Sigma^-$	$7\sigma^2 \rightarrow 3\pi^2$	9.94	0
1	$X^1\Sigma^+$	$\cdots 2\pi^4 11\sigma^2 3\pi^4 4\pi^0$	0.00	
	$1^1\Pi$	$11\sigma \rightarrow 4\pi$	3.20	1.46×10^{-2}
	$1^1\Sigma^-$	$3\pi \rightarrow 4\pi$	3.24	0
	$1^1\Delta$	$3\pi \rightarrow 4\pi$	3.24	0
	$2^1\Delta$	$2\pi \rightarrow 4\pi$	5.93	0
	$2^1\Sigma^-$	$2\pi \rightarrow 4\pi$	5.94	0
	$2^1\Sigma^+$	$3\pi^2 \rightarrow 4\pi^2$	6.14	6.16×10^{-3}
	$2^1\Pi$	$11\sigma 3\pi \rightarrow 4\pi^2$	6.62	4.99×10^{-4}
2	$X^1\Sigma^+$	$\cdots 3\pi^4 15\sigma^2 4\pi^4 5\pi^0$	0.00	
	$1^1\Sigma^-$	$4\pi \rightarrow 5\pi$	2.17	0
	$1^1\Delta$	$4\pi \rightarrow 5\pi$	2.18	0
	$1^1\Pi$	$15\sigma \rightarrow 5\pi$	2.50	6.71×10^{-3}
	$2^1\Sigma^-$	$3\pi \rightarrow 5\pi$	4.30	0
	$2^1\Delta$	$3\pi \rightarrow 5\pi$	4.32	0
	$2^1\Sigma^+$	$4\pi^2 \rightarrow 5\pi^2$	4.47 (4.36)[b]	1.47×10^{-4}
	$2^1\Pi$	$15\sigma 4\pi \rightarrow 5\pi^2$	4.77	3.61×10^{-5}
3	$X^1\Sigma^+$	$\cdots 4\pi^4 19\sigma^2 5\pi^4 6\pi^0$	0.00	
	$1^1\Delta$	$5\pi \rightarrow 6\pi$	1.56	0
	$1^1\Sigma^-$	$5\pi \rightarrow 6\pi$	1.57	0
	$1^1\Pi$	$19\sigma \rightarrow 6\pi$	1.72	3.68×10^{-3}
	$2^1\Sigma^-$	$4\pi \rightarrow 6\pi$	3.27	0
	$2^1\Delta$	$4\pi \rightarrow 6\pi$	3.30	0
	$2^1\Sigma^+$	$5\pi^2 \rightarrow 6\pi^2$	3.38	2.18×10^{-4}
	$2^1\Pi$	$19\sigma 5\pi \rightarrow 6\pi^2$	3.78	8.95×10^{-6}
4	$X^1\Sigma^+$	$\cdots 5\pi^4 23\sigma^2 6\pi^4 7\pi^0$	0.00	
	$1^1\Delta$	$6\pi \rightarrow 7\pi$	1.28	0
	$1^1\Sigma^-$	$6\pi \rightarrow 7\pi$	1.31	0
	$1^1\Pi$	$23\sigma \rightarrow 7\pi$	2.18	4.83×10^{-3}
	$2^1\Sigma^-$	$5\pi \rightarrow 7\pi$	2.65	0
	$2^1\Delta$	$5\pi \rightarrow 7\pi$	2.67	0
	$2^1\Sigma^+$	$6\pi^2 \rightarrow 7\pi^2$	2.79	6.98×10^{-5}
	$2^1\Pi$	$23\sigma 6\pi \rightarrow 7\pi^2$	3.75	1.51×10^{-5}

[a] Experimental value from ref 22. [b] Experimental value from ref 22.

the electronic promotion from 2π to 3π are 5.73 and 5.80 eV higher in energy than the ground state, respectively. The strongest $2^1\Sigma^+\leftarrow X^1\Sigma^+$ transition from $2\pi \rightarrow 3\pi$ electronic promotion occurs at 8.14 eV, with $f = 1.52 \times 10^{-1}$. The $2^1\Pi$ state mainly contributed by the $2\pi 7\sigma \rightarrow 3\pi^2$ double excitation is placed at 9.01 eV above the ground state, with $f = 9.01 \times 10^{-2}$. The $7\sigma^2 \rightarrow 3\pi^2$ double excitation gives rise to low-lying states $3^1\Sigma^+$ and $2^1\Sigma^-$ at 9.77 ($f = 3.59 \times 10^{-3}$) and 9.94 eV ($f = 0$), respectively.

For $C_{2n+1}S$ ($n = 1-4$), the HOMO−LUMO single excitation leads to the $1^1\Sigma^-$ and $1^1\Delta$ states, which are nearly degenerate. The $2^1\Sigma^-$ and $2^1\Delta$ states, derived from electronic transition from HOMO-2 (π) to LUMO, are also nearly degenerate. The allowed

$2^1\Sigma^+ \leftarrow X^1\Sigma^+$ transitions are double electronic excitations from HOMO to LUMO. The electronic promotion from $(4n+7)\sigma$ to $(n+3)\pi$ will result in the $1^1\Pi$ state, while the higher $2^1\Pi$ state arises from the $(4n + 7)\sigma\ (n + 2)\pi \rightarrow (n + 3)\pi^2$ double excitation. As shown in Table 4, the $^1\Delta \leftarrow X^1\Sigma^+$ and $^1\Sigma^- \leftarrow X^1\Sigma^+$ transitions are dipole forbidden with $f = 0$, while the $^1\Pi \leftarrow X^1\Sigma^+$ and $^1\Sigma^+ \leftarrow X^1\Sigma^+$ transitions are dipole allowed to appear in the electronic absorption spectra, with f in the magnitude of $10^{-2}-10^{-6}$.

As n increases, the vertical excitation energies of corresponding low-lying states in $C_{2n+1}S$ ($n = 1-4$) decrease gradually. To examine the size dependence of the singlet−singlet transition energies, an exponential-decay curve fitting has been performed using calculated vertical transition energies (ΔE in eV). For the $2^1\Sigma^+ \leftarrow X^1\Sigma^+$ transition, this fitting gives the following equation:

$$\Delta E = 1.7785 + 9.13499e^{-n/4.06439} \quad (2)$$

The fitting error and correlation coefficient are 0.00163 and 0.99975, respectively, showing high accuracy. Equation 2 indicates a nonlinear dependence of the vertical transition energies on the chain size, and it will converge to the limit of about 1.78 eV as the chain size approaches infinite.

Energies of Singlet Excited States in $C_{2n+1}Cl^+$. The linear $C_{2n+1}Cl^+$ ($n = 0-4$) clusters have the same electronic configurations as their isoelectonic series $C_{2n+1}S$. Similarly, they have the ground state of $X^1\Sigma^+$. The selected vertical excitation energies (ΔE) and oscillator strengths (f) of the low-lying singlet excited states in $C_{2n+1}Cl^+$ ($n = 0-4$) are presented in Table 5. Available experimental values are presented in Table 5 for comparison.

Calculations show that the lowest excited state $1^1\Pi$ of CCl^+, arising from $7\sigma \rightarrow 3\pi$ excitation, lies at 5.35 eV above the ground state, with an oscillator strength of 2.35×10^{-2}. Next low-lying states $1^1\Delta$ and $1^1\Sigma^-$ from the $2\pi \rightarrow 3\pi$ electronic excitation are 6.44 and 6.74 eV higher in energy than the ground state, respectively. The strongest $2^1\Sigma^+ \leftarrow X^1\Sigma^+$ transition occurs at 8.57 eV ($f = 1.13 \times 10^{-1}$), and it is also derived from the $2\pi \rightarrow 3\pi$ electronic excitation. The $2^1\Pi$ state, derived from the $2\pi 7\sigma \rightarrow 3\pi^2$ double excitation, is 10.26 eV ($f = 2.76 \times 10^{-2}$) above the ground state. The $7\sigma^2 \rightarrow 3\pi^2$ double excitation, i.e., the HOMO−LUMO electron promotion, gives rise to the low-lying states $2^1\Delta$ and $2^1\Sigma^-$, lying at 10.26 ($f = 0$) and 10.54 eV ($f = 0$), respectively.

For C_3Cl^+, the lowest excited state is $1^1\Pi$, arising from the $11\sigma \rightarrow 4\pi$ excitation, i.e., the HOMO−LUMO electronic promotion, lies at 2.89 eV ($f = 1.21 \times 10^{-2}$) above the ground state, in agreement with experimental value of 3.00 eV.[35] The electronic promotion from 3π to 4π leads to the $1^1\Sigma^-$ and $1^1\Delta$ states. The $2\pi \rightarrow 4\pi$ electronic excitation will result in higher-energy $2^1\Sigma^-$ and $2^1\Delta$ states. The $2^1\Pi$ state from the $3\pi 11\sigma \rightarrow 4\pi^2$ double excitation is placed at 6.36 eV above the ground state. The allowed $2^1\Sigma^+ \leftarrow X^1\Sigma^+$ transition from the $3\pi^2 \rightarrow 4\pi^2$ double excitation occurs at 7.17 eV ($f = 1.05 \times 10^{-1}$).

Like C_3Cl^+, C_5Cl^+ exhibits similar properties of the low-lying excited states. The first excited state $1^1\Pi$ lies at 2.34 eV ($f = 7.99 \times 10^{-3}$). The relatively strong $2^1\Sigma^+ \leftarrow X^1\Sigma^+$ transition occurs at 5.09 eV, which is comparable with the experimental value.[36] For C_7Cl^+ and C_9Cl^+, the electronic promotion from HOMO to LUMO ($\pi \rightarrow$ p) leads to the low-lying states of $1^1\Sigma^-$, $1^1\Delta$, and $2^1\Sigma^+$; the electronic excitation from HOMO-1 to LUMO ($\sigma \rightarrow$ p) gives rise to $1^1\Pi$; the electronic elevation from HOMO-2 to LUMO ($\pi \rightarrow$ p) results in $2^1\Sigma^-$ and $2^1\Delta$. All of these excited states arise from single excitations. The $(4n + 7)\sigma\ (n + 2)\pi \rightarrow (n + 3)\pi^2$ double excitations yield a $2^1\Pi$ state.

TABLE 5: Calculated Vertical Excitation Energies ΔE (in eV) and Oscillator Strengths f of the Singlet Excited States in $C_{2n+1}Cl^+$ ($n = 0-4$) by CASPT2

n	state	transition	ΔE	f
0	$X^1\Sigma^+$	$\cdots 2\pi^4 7\sigma^2 3\pi^0$		
	$1^1\Pi$	$7\sigma \rightarrow 3\pi$	5.35	2.35×10^{-2}
	$1^1\Delta$	$2\pi \rightarrow 3\pi$	6.44	0
	$1^1\Sigma^-$	$2\pi \rightarrow 3\pi$	6.74	0
	$2^1\Sigma^+$	$2\pi \rightarrow 3\pi$	8.57	1.13×10^{-1}
	$2^1\Pi$	$2\pi 7\sigma \rightarrow 3\pi^2$	10.26	2.76×10^{-2}
	$2^1\Delta$	$7\sigma^2 \rightarrow 3\pi^2$	10.26	0
	$2^1\Sigma^-$	$7\sigma^2 \rightarrow 3\pi^2$	10.54	0
1	$X^1\Sigma^+$	$\cdots 2\pi^4 3\pi^4 11\sigma^2 4\pi^0$		
	$1^1\Pi$	$11\sigma \rightarrow 4\pi$	2.89 (3.00)[a]	1.21×10^{-2}
	$1^1\Sigma^-$	$3\pi \rightarrow 4\pi$	3.56	0
	$1^1\Delta$	$3\pi \rightarrow 4\pi$	3.86	0
	$2^1\Pi$	$3\pi 11\sigma \rightarrow 4\pi^2$	6.36	2.58×10^{-5}
	$2^1\Sigma^-$	$2\pi \rightarrow 4\pi$	6.71	0
	$2^1\Sigma^+$	$2\pi \rightarrow 4\pi$	6.73	7.00×10^{-1}
	$3^1\Sigma^+$	$3\pi^2 \rightarrow 4\pi^2$	7.07	1.39×10^{-1}
	$2^1\Delta$	$2\pi \rightarrow 4\pi$	7.39	0
2	$X^1\Sigma^+$	$\cdots 3\pi^4 15\sigma^2 4\pi^4 5\pi^0$		
	$1^1\Pi$	$15\sigma \rightarrow 5\pi$	2.34	7.99×10^{-3}
	$1^1\Sigma^-$	$4\pi \rightarrow 5\pi$	2.67	0
	$1^1\Delta$	$4\pi \rightarrow 5\pi$	2.69	0
	$2^1\Sigma^-$	$3\pi \rightarrow 5\pi$	4.93	0
	$2^1\Delta$	$3\pi \rightarrow 5\pi$	4.97	0
	$2^1\Pi$	$15\sigma 4\pi \rightarrow 5\pi^2$	5.01	1.13×10^{-6}
	$2^1\Sigma^+$	$4\pi^2 \rightarrow 5\pi^2$	5.09 (4.66)[b]	4.42×10^{-3}
3	$X^1\Sigma^+$	$\cdots 4\pi^4 19\sigma^2 5\pi^4 6\pi^0$		
	$1^1\Pi$	$19\sigma \rightarrow 6\pi$	1.65	5.61×10^{-3}
	$1^1\Sigma^-$	$5\pi \rightarrow 6\pi$	1.99	0
	$1^1\Delta$	$5\pi \rightarrow 6\pi$	2.08	0
	$2^1\Sigma^+$	$5\pi \rightarrow 6\pi$	3.31	1.3698
	$2^1\Pi$	$19\sigma 5\pi \rightarrow 6\pi^2$	3.72	4.74×10^{-7}
	$2^1\Sigma^-$	$4\pi \rightarrow 6\pi$	3.83	0
	$2^1\Delta$	$4\pi \rightarrow 6\pi$	3.93	0
4	$X^1\Sigma^+$	$\cdots 5\pi^4 23\sigma^2 6\pi^4 7\pi^0$		
	$1^1\Sigma^-$	$6\pi \rightarrow 7\pi$	1.46	0
	$1^1\Delta$	$6\pi \rightarrow 7\pi$	1.52	0
	$1^1\Pi$	$23\sigma \rightarrow 7\pi$	1.75	5.86×10^{-3}
	$2^1\Sigma^+$	$6\pi \rightarrow 7\pi$	2.51	1.4877
	$2^1\Sigma^-$	$5\pi \rightarrow 7\pi$	2.57	0
	$2^1\Delta$	$5\pi \rightarrow 7\pi$	2.60	0
	$2^1\Pi$	$23\sigma 6\pi \rightarrow 7\pi^2$	3.54	1.52×10^{-7}

[a] Observed value from ref 35. [b] Observed value from ref 36.

As Table 5 displays, the strongest transitions correspond to $2^1\Sigma^+ \leftarrow X^1\Sigma^+$ in both C_7Cl^+ and C_9Cl^+ with large oscillator strengths of 1.3698 and 1.4877, respectively. Such strong electronic transitions arise from the $(n + 2)\pi \rightarrow (n + 3)\pi$ single excitation, whereas similar electronic excitation has not been found in low-lying states of other chains considered here.

C. Vertical Excitation Energies of Triplet States. The calculated relative energies of the low-lying triplet excited states for $C_{2n+1}S$ and $C_{2n+1}Cl^+$ ($n = 1-4$) are displayed in Tables 6 and 7. Notice that the relative energy level has a similar pattern and all of these transitions mainly arise from single excitations. The low-energy excited states are $1^3\Sigma^+$, $1^3\Delta$ and $1^3\Sigma^-$, arising from the HOMO−LUMO ($\pi-\pi$) excitation. Next low-lying states are $2^3\Sigma^+$, $2^3\Delta$, and $2^3\Sigma^-$, derived from the electron promotion from the next highest occupied π orbital to LUMO. Generally, the excited states of $C_{2n+1}S$ are lower in energy than corresponding those of $C_{2n+1}Cl^+$.

To examine accessibility of the spin-forbidden triplet excited states, SOC−CI calculations have been carried out for the low-lying triplet excited states. As shown in Tables 6 and 7, the oscillator strengths for spin-forbidden $1^3\Sigma^- \leftarrow X^1\Sigma^+$ and $2^3\Sigma^- \leftarrow X^1\Sigma^+$ transitions are in the magnitude of $10^{-6}-10^{-8}$, while the oscillator strengths for other transitions considered here are vanishing.

TABLE 6: Calculated Vertical Excitation Energies ΔE (in eV) and Oscillator Strengths *f* of the Triplet Excited States in $C_{2n+1}S$ ($n = 1-4$) by CASPT2

n	electronic state	transition	ΔE	f
1	$X^1\Sigma^+$	$\cdots 2\pi^4 11\sigma^2 3\pi^4 4\pi^0$	0.00	
	$1^3\Sigma^+$	$3\pi \rightarrow 4\pi$	2.74	0
	$1^3\Delta$	$3\pi \rightarrow 4\pi$	3.05	0
	$1^3\Sigma^-$	$3\pi \rightarrow 4\pi$	3.27	1.64×10^{-8}
	$2^3\Sigma^+$	$2\pi \rightarrow 4\pi$	5.17	0
	$2^3\Delta$	$2\pi \rightarrow 4\pi$	5.56	0
	$2^3\Sigma^-$	$2\pi \rightarrow 4\pi$	5.77	1.67×10^{-7}
2	$X^1\Sigma^+$	$\cdots 3\pi^4 15\sigma^2 4\pi^4 5\pi^0$	0.00	
	$1^3\Sigma^+$	$4\pi \rightarrow 5\pi$	1.88	0
	$1^3\Delta$	$4\pi \rightarrow 5\pi$	2.06	0
	$1^3\Sigma^-$	$4\pi \rightarrow 5\pi$	2.18	1.37×10^{-8}
	$2^3\Sigma^+$	$3\pi \rightarrow 5\pi$	3.80	0
	$2^3\Delta$	$3\pi \rightarrow 5\pi$	4.04	0
	$2^3\Sigma^-$	$3\pi \rightarrow 5\pi$	4.17	4.73×10^{-7}
3	$X^1\Sigma^+$	$\cdots 4\pi^4 19\sigma^2 5\pi^4 6\pi^0$	0.00	
	$1^3\Sigma^+$	$5\pi \rightarrow 6\pi$	1.43	0
	$1^3\Delta$	$5\pi \rightarrow 6\pi$	1.53	0
	$1^3\Sigma^-$	$5\pi \rightarrow 6\pi$	1.60	1.58×10^{-8}
	$2^3\Sigma^+$	$4\pi \rightarrow 6\pi$	2.90	0
	$2^3\Delta$	$4\pi \rightarrow 6\pi$	3.08	0
	$2^3\Sigma^-$	$4\pi \rightarrow 6\pi$	3.17	3.60×10^{-7}
4	$X^1\Sigma^+$	$\cdots 5\pi^4 23\sigma^2 6\pi^4 7\pi^0$	0.00	
	$1^3\Sigma^+$	$6\pi \rightarrow 7\pi$	1.10	0
	$1^3\Delta$	$6\pi \rightarrow 7\pi$	1.17	
	$1^3\Sigma^-$	$6\pi \rightarrow 7\pi$	1.21	1.24×10^{-8}
	$2^3\Sigma^+$	$5\pi \rightarrow 7\pi$	2.21	0
	$2^3\Delta$	$5\pi \rightarrow 7\pi$	2.37	0
	$2^3\Sigma^-$	$5\pi \rightarrow 7\pi$	2.44	3.52×10^{-7}

TABLE 7: Calculated Vertical Excitation Energies ΔE (in eV) and Oscillator Strengths *f* of the Triplet Excited States in $C_{2n+1}Cl^+$ ($n = 1-4$) by CASPT2

n	state	transition	ΔE	f
1	$X^1\Sigma^+$	$\cdots 2\pi^4 3\pi^4 11\sigma^2 4\pi^0$		
	$1^3\Sigma^+$	$3\pi \rightarrow 4\pi$	3.00	0
	$1^3\Delta$	$3\pi \rightarrow 4\pi$	3.36	0
	$1^3\Sigma^-$	$3\pi \rightarrow 4\pi$	3.53	8.67×10^{-7}
	$2^3\Sigma^+$	$2\pi \rightarrow 4\pi$	6.12	0
	$2^3\Delta$	$2\pi \rightarrow 4\pi$	6.45	0
	$2^3\Sigma^-$	$2\pi \rightarrow 4\pi$	6.64	6.67×10^{-6}
2	$X^1\Sigma^+$	$\cdots 3\pi^4 15\sigma^2 4\pi^4 5\pi^0$		
	$1^3\Sigma^+$	$4\pi \rightarrow 5\pi$	2.26	0
	$1^3\Delta$	$4\pi \rightarrow 5\pi$	2.52	0
	$1^3\Sigma^-$	$4\pi \rightarrow 5\pi$	2.68	1.21×10^{-7}
	$2^3\Sigma^+$	$3\pi \rightarrow 5\pi$	4.31	0
	$2^3\Delta$	$3\pi \rightarrow 5\pi$	4.65	0
	$2^3\Sigma^-$	$3\pi \rightarrow 5\pi$	4.83	1.14×10^{-7}
3	$X^1\Sigma^+$	$\cdots 4\pi^4 19\sigma^2 5\pi^4 6\pi^0$		
	$1^3\Sigma^+$	$5\pi \rightarrow 6\pi$	1.67	0
	$1^3\Delta$	$5\pi \rightarrow 6\pi$	1.86	0
	$1^3\Sigma^-$	$5\pi \rightarrow 6\pi$	1.99	1.34×10^{-7}
	$2^3\Sigma^+$	$4\pi \rightarrow 6\pi$	3.33	0
	$2^3\Delta$	$4\pi \rightarrow 6\pi$	3.58	0
	$2^3\Sigma^-$	$4\pi \rightarrow 6\pi$	3.74	2.75×10^{-7}
4	$X^1\Sigma^+$	$\cdots 5\pi^4 23\sigma^2 6\pi^4 7\pi^0$		
	$1^3\Sigma^+$	$6\pi \rightarrow 7\pi$	1.23	0
	$1^3\Delta$	$6\pi \rightarrow 7\pi$	1.38	0
	$1^3\Sigma^-$	$6\pi \rightarrow 7\pi$	1.46	1.25×10^{-7}
	$2^3\Sigma^+$	$5\pi \rightarrow 7\pi$	2.23	0
	$2^3\Delta$	$5\pi \rightarrow 7\pi$	2.41	0
	$2^3\Sigma^-$	$5\pi \rightarrow 7\pi$	2.50	3.00×10^{-7}

Interestingly, the spin-forbidden $1^3\Sigma^- \leftarrow X^1\Sigma^+$ transition in $C_{2n+1}Cl^+$ has relatively large oscillator strength with respect to $C_{2n+1}S$, while the oscillator strengths of $2^3\Sigma^- \leftarrow X^1\Sigma^+$ transitions are comparable for both species. Note that the even-numbered carbon chains $C_{2n}S$ and $C_{2n}Cl^+$ have notable reactivity for spin-forbidden transitions.[37] Such distinct accessibilities of the spin-forbidden excited states suggest that effects of spin−orbit coupling on the spin-forbidden transitions have geometrical and electronic structural dependence.

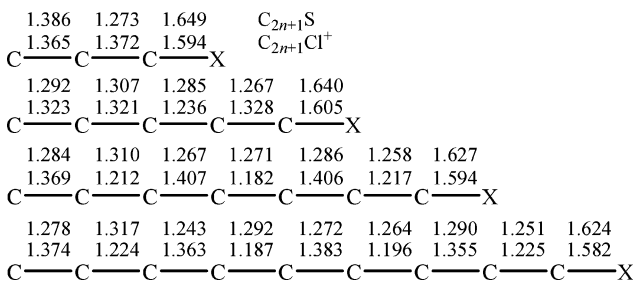

Figure 3. CASSCF-optimized geometries (in Å) of the excited states $2^1\Sigma^+$ for $C_{2n+1}S$ and $C_{2n+1}Cl^+$.

TABLE 8: Vertical Emission Energies ΔE (in eV) and Corresponding Transition Moments (|TM| in au) for the $2^1\Sigma^+ \rightarrow X^1\Sigma^+$ Transition of $C_{2n+1}S$ and $C_{2n+1}Cl^+$ ($n = 1-4$)

$C_{2n+1}S$	ΔE	|TM|	$C_{2n+1}Cl^+$	ΔE	|TM|
$n = 1$	5.23	0.5598	$n = 1$	6.09	1.0304
$n = 2$	4.28	0.1527	$n = 2$	4.37	0.4767
$n = 3$	3.33	0.1030	$n = 3$	2.81	3.9050
$n = 4$	2.67	0.0426	$n = 4$	2.17	4.7421

D. Vertical Emission Energies of $2^1\Sigma^+$. The CASSCF-optimized geometries of the $2^1\Sigma^+$ excited states in linear chains $C_{2n+1}S$ and $C_{2n+1}Cl^+$ ($n = 1-4$) are shown in Figure 3. As Figure 3 shows, the bond lengths of C−S and C−Cl in $C_{2n+1}S$ and $C_{2n+1}Cl^+$ gradually decrease as the chain size increases except C_3Cl^+. Like their ground states, the $2^1\Sigma^+$ excited states have the dominant character of cumulenic structure in $C_{2n+1}S$ and a striking character of acetylenic structure in $C_{2n+1}Cl^+$.

On the basis of these optimized geometries of the $2^1\Sigma^+$ states, the vertical emission energies for the $2^1\Sigma^+ \rightarrow X^1\Sigma^+$ transition in linear $C_{2n+1}S$ and $C_{2n+1}Cl^+$ ($n = 1-4$) have been calculated by the CASPT2 method. Predicted emission energies are listed in Table 8. The corresponding state-state transition dipole moments (TM) have been estimated, and they can be served as an approximate measurement for emission yield.

As Tables 4, 5, and 8 show, the vertical emissions of the $2^1\Sigma^+$ states exhibit less red shift due to relaxation of the excited state with respect to their corresponding absorption spectra. The red-shift magnitude decreases with the increase of chain. For $C_{2n+1}S$, as the chain size *n* increases from 1 to 4, the vertical emission energy decreases from 5.23 to 2.67 eV gradually. Like $C_{2n+1}S$, the vertical emission energy in $C_{2n+1}Cl^+$ decreases from 6.09 to 2.17 eV with the increase of chain.

IV. Conclusions

The equilibrium structures of the isoelectronic systems $C_{2n+1}S$ and $C_{2n+1}Cl^+$ ($n = 0-4$) in their ground states have been investigated by B3LYP and CCSD calculations. Calculations show that these heteroatom-containing chains have stable linear structures in the $X^1\Sigma^+$ states, and the optimized geometries show good agreement with available experimental values. The predicted dipole moments of both $C_{2n+1}S$ and $C_{2n+1}Cl^+$ increase linearly as the chain lengthens. Generally, the $C_{2n+1}S$ cluster has larger dipole moments than corresponding $C_{2n+1}Cl^+$.

At the CASPT2 level of theory, the selected low-lying excited states have been studied. For $C_{2n+1}S$ ($n = 1-4$) and $C_{2n+1}Cl^+$ ($n = 1, 2$), all the $2^1\Sigma^+$ states arise from the highest occupied π orbital to LUMO double excitation, while for $C_{2n+1}Cl^+$ ($n = 3, 4$), the $2^1\Sigma^+ \leftarrow X^1\Sigma^+$ transitions correspond to the HOMO−LUMO ($\pi-\pi$) single excitation. Both isoelectronic series exhibit similar size dependences of absorption and emission spectra.

In particular, the vertical excitation energy for relatively strong $2^1\Sigma^+ \leftarrow X^1\Sigma^+$ transition in $C_{2n+1}S$ has nonlinear size dependence of an exponential-decay relationship. The CASPT2 calculations indicate that strong $1^1\Pi \leftarrow X^1\Sigma^+$ transitions in CS and C_3Cl^+ occur at 4.92 and 2.89 eV, respectively, and strong $2^1\Sigma^+ \leftarrow X^1\Sigma^+$ transitions in C_5S and C_5Cl^+ appear at 4.47 and 5.09 eV, respectively, which are in reasonably agreement with the corresponding observed values of 4.81, 3.00, 4.36, and 4.66 eV.

On the basis of SOC−CI calculations, the effect of spin−orbit coupling on the spin-forbidden electronic transition has been discussed. The results show that the oscillator strengths for singlet−triplet transitions are generally very small and these excited triplet states considered here in both isoelectronic series are less accessible by direct singlet−triplet transitions. The effect of spin−orbit coupling on the spin-forbidden transition indicates geometrical and electronic structural dependence.

Acknowledgment. This project is supported by the State Key Laboratory of Physical Chemistry of Solid Surfaces (No. 200306), the Natural Science Foundation of Henan Province (Nos. 0311011200 and 200510475012), the National Natural Science Foundation (Nos. 20473062, 20233020, 20021002, and 20173042), and the Ministry of Science and Technology (Nos. 2004CB719902 and 001CB1089).

References and Notes

(1) Kushmerick, J. G.; Naciri, J.; Yang, J. C.; Shashidhar, R. *Nano. Lett.* **2003**, *3*, 897.
(2) Joachim, C.; Gimzewski, J. K.; Aviram, A. *Nature* **2000**, *408*, 541.
(3) Cui, X. D.; Primak, A.; Zarate, X.; Tomfohr, J.; Sankey, O. F.; Moore, A. L.; Moore, T. A.; Gust, D.; Harris, G.; Lindsay, S. M. *Science* **2001**, *294*, 571.
(4) Fan, F. F.; Yao, Y.; Cai, L.; Cheng, L.; Tour, J. M.; Bard, A. J. *J. Am. Chem. Soc.* **2004**, *126*, 4035.
(5) Robertson N.; McGowan, C. A. *Chem. Soc. Rev.* **2003**, *32*, 96.
(6) Welter, W., Jr.; Van Zee, R. J. *Chem. Rev.* **1989**, *89*, 1713.
(7) Parent, D. C.; Anderson, S. L. *Chem. Rev.* **1992**, *92*, 1541.
(8) Orden, A. V.; Saykally, R. J. *Chem. Rev.* **1998**, *98*, 2313.
(9) Pascoli, G.; Lavendy, H. *Int. J. Mass Spectrosc.* **2001**, *206*, 153.
(10) Hinkle, K. H.; Keady, J. J.; Bernath, P. F. *Science* **1988**, *241*, 1319.
(11) Bernath, P. F.; Hinkle, K. H.; Keady, J. J. *Science* **1989**, *244*, 562.
(12) Henning, Th.; Salama, F. *Science* **1998**, *282*, 2204.
(13) Millar, T. J.; Herbst, E. *Astrophys. Astron.* **1990**, *231*, 466.
(14) Gordon, V. D.; McCarthy, M. C.; Apponi, A. J.; Thaddeus, P. *Astrophys. J. Suppl.* **2001**, *134*, 311.
(15) Szczepanski, J.; Hodyss, R.; Fuller, J.; Vala, M. *J. Phys. Chem. A* **1999**, *103*, 2975.
(16) Lee, S. *Chem. Phys. Lett.* **1997**, *268*, 69.
(17) Wang, H.; Szczepanski, J.; Brucat, P.; Vala, M. *Inter. J. Quantum Chem.* **2005**, *102*, 795.
(18) Wang, H.; Szczepanski, J.; Cooke, A.; Brucat, P.; Vala, M. *Inter. J. Quantum Chem.* **2005**, *102*, 806.
(19) Schoeffler, A. J.; Kohguchi, H.; Hoshina, K.; Ohshima, Y.; Endo, Y. *J. Chem. Phys.* **2001**, *114*, 6142.
(20) Riaplov, E.; Wyss, M.; Maier, J. P.; Panten, D.; Chambaud, G.; Rosmus, P.; Fabian, J. *J. Mol. Spectrosc.* **2003**, *222*, 15.
(21) Riaplov, E.; Wyss, M.; Lakin, N. M.; Maier, J. P. *J. Phys. Chem. A* **2001**, *105*, 4894.
(22) Riaplov, E.; Maier, J. P. *J. Phys. Chem. A* **2003**, *107*, 8856.
(23) Venkateswarlu, P.; *Phys. Rev.* **1950**, *77*, 79.
(24) Verma, R. D.; Mulliken, R. S. *J. Mol. Spectrosc.* **1961**, *6*, 419.
(25) Gordon, R. D.; King, G. W. *Can. J. Phys.* **1961**, *39*, 252.
(26) Endo, Y.; Saito, S.; Hirota, E. *J. Mol. Spectrosc.* **1982**, *94*, 199.
(27) Yamada, C.; Nagai, K.; Hirota, E. *J. Mol. Spectrosc.* **1981**, *85*, 416.
(28) Burkholder, J. B.; Sinha, A.; Hammer, P. D.; Howard, C. J. *J. Mol. Spectrosc.* **1988**, *127*, 61.
(29) Jin, P.; Chang, B. C.; Fei, R.; Sears, T. J. *J. Mol. Spectrosc.* **1997**, *182*, 189.
(30) Bredohl, H.; Dubois, I.; Melen, F. *J. Mol. Spectrosc.* **1983**, *98*, 495.
(31) Sumiyohsi, Y.; Ueno, T.; Endo, Y. *J. Chem. Phys.* **2003**, *119*, 1426.
(32) Redondo, P.; Redondo, J. R.; Barrientos, C.; Largo, A. *Chem. Phys. Lett.* **1999**, *315*, 224.
(33) Largo, A.; Cimas, A.; Redondo, P.; Barrientos, C. *Int. J. Quantum Chem.* **2001**, *84*, 127.
(34) Li, G.; Tang, Z. *J. Phys. Chem. A* **2003**, *107*, 5317.
(35) Wijngaarden, J. V.; Shnitko, I.; Batalov, A.; Kolek, P.; Fulara, J.; Maier, J. P. *J. Phys. Chem. A* **2005**, *109*, 5553.
(36) Wijngaarden, J. V.; Batalov, A.; Shnitko, I.; Fulara, J.; Maier, J. P. *J. Phys. Chem. A* **2004**, *108*, 4219.
(37) Zhang, J.; Wu, W.; Wang, L.; Cao, Z. *J. Chem. Phys.* **2006**, *124*, 124319.
(38) (a) Knowles, P. J.; Hampel, C.; Werner, H.-J. *J. Chem. Phys.* **1993**, *99*, 5219. (b) Cizek, J. *Adv. Chem. Phys*. **1969**, *14*, 35. (c) Purvis, G. D.; Bartlett, R. J. *J. Chem. Phys.* **1982**, *76*, 1910. (d) Scuseria, G. E.; Janssen, C. L.; Schaefer, H. F., III, *J. Chem. Phys.* **1988**, *89*, 7382.
(39) Lee, C.; Yang, W.; Parr, R. G. *Phys. Rev. B* **1988**, *37*, 785.
(40) Miehlich, B.; Savin, A.; Stoll, H.; Preuss, H. *Chem. Phys. Lett.* **1989**, *157*, 200.
(41) Becke, A. D. *J. Chem. Phys.* **1993**, *98*, 5648.
(42) Celani, P.; Werner, H.-J. *J. Chem. Phys.* **2000**, *112*, 5546.
(43) Berning, A.; Schweizer, M.; Werner, H.-J.; Knowles, P. J.; Palmieri, P. *Mol. Phys.* **2000**, *98*, 1823.
(44) Werner, H.-J.; Knowles, P. J. *J. Chem. Phys.* **1985**, *82*, 5053.
(45) Knowles, P. J.; Werner, H.-J. *Chem. Phys. Lett.* **1985**, *115*, 259.
(46) Frisch, M. J.; Trucks, G. W.; Schegel, H. B.; Scuseria, G. E.; Robb, M. A.; Cheeseman, J. R.; Zakrzewski, V. G.; Montgomery, J. A., Jr.; Stratmann, R. E.; Burant, J. C.; Dapprich, S.; Millam, J. M.; Daniels, A. D.; Kudin, K. N.; Strain, M. C.; Farkas, O.; Tomasi, J.; Barone, V.; Cossi, M.; Cammi, R.; Mennucci, B.; Pomelli, C.; Adamo, C.; Clifford, S.; Ochterski, J.; Peterson, G. A.; Ayala, P. Y.; Cui, Q.; Morokuma, K.; Malick, D. K.; Raghavachari, K.; Foresman, J. B.; Cioslowski, J.; Ortiz, J. V.; Sefanov, B. B.; Liu, G.; Liashenko, A.; Piskorz, P.; Komaromi, I.; Gomperts, R.; Martin, R. L.; Fox, D. J.; Keith, T.; Al-Laham, M. A.; Peng, C. Y.; Nanayakkara, A.; Gonzalez, C.; Chahacombe, M.; Gill, P. M. W.; Johnson, B. G.; Chen, W.; Wong, M. W.; Andres, J. L.; Gonzalez, C.; Head-Gordon, M.; Replogle, E. S.; Pople, J. A. *Gaussian 98*, Revision A.11; Gaussian Inc.: Pittsburgh, PA, 2001.
(47) *(47) MOLPRO, a package of ab initio* programs designed by Werner H.-J.; Knowles P. J., version 2002.1. Amos, R. D.; Bernhardsson, A.; Berning, A.; Celani, P.; Cooper, D. L.; Deegan, M. J. O.; Dobbyn, A. J.; Eckert, F.; Hampel, C.; Hetzer, G..; Knowles, P. J.; Korona, T.; Lindh, R.; Lloyd, A. W.; McNicholas, S. J.; Manby, F. R.; Meyer, W.; Mura, M. E.; Nicklass, A.; Palmieri, P.; Pitzer, R.; Rauhut, G.; Schütz, M.; Schumann, U.; Stoll, H.; Stone, A. J.; Tarroni, R.; Thorsteinsson, T.; Werner, H.-J.
(48) Ohshima, Y.; Endo, Y. *J. Mol. Spectrosc.* **1992**, *153*, 627.
(49) Bogey, M.; Demuynck, C.; Destombes, J. L. *J. Mol. Spectrosc.* **1982**, *95*, 15.
(50) Zhang, J.; Wang, L.; Wu, W.; Cao, Z. *Acta Phys.-Chim. Sin.* **2004**, *20*, 1428 (in Chinese).
(51) Burnin, A.; BelBruno, J. J. *J. Phys. Chem. A* **2003**, *107*, 9547.
(52) Yamamoto, S.; Saito, S.; Kawaguchi, K.; Kaifu, N.; Suzuki, H.; Ohishi, M. *Astrophys. J.* **1987**, *317*, L119.
(53) Saito, S.; Kawaguchi, K.; Yamamoto, S.; Ohishi, M.; Suzuki, H.; Kaifu, N. *Astrophys. J.* **1987**, *317*, L115.
(54) Yamamoto, S.; Saito, S.; Kawaguchi, K.; Chicada, Y.; Suzuki, H.; Kaifu, N.; Ishikawa, S. *Astrophys. J.* **1990**, *361*, 318.
(55) Hirahara, Y.; Ohshima, Y.; Endo, Y. *Astrophys. J.* **1993**, *408*, L113.
(56) Kasai, Y.; Obi, K.; Ohshima, Y.; Hirahara, Y.; Endo, Y.; Kawaguchi, K.; Murakami, A. *Astrophys. J.* **1993**, *410*, L45.
(57) Maier, G.; Schrot, J.; Reisenauer, H. P.; Janoschek, R. *Chem. Ber.* **1991**, *124*, 2617.
(58) Maier, G.; Schrot, J.; Reisenauer, H. P. *Chem. Ber.* **1991**, *124*, 2613.
(59) Maier, G.; Schrot, J.; Reisenauer, H. P.; Janoschek, R. *Chem. Ber.* **1990**, *123*, 1753.
(60) Wijngaarden, J. V.; Shnitko, I.; Batalov, A.; Kolek, P.; Fulara, J.; Maier, J. P. *J. Phys. Chem. A* **2005**, *109*, 5553.